APPLIED MATHEMATICS AND MECHANICS (ENGLISH EDITION)

Molybdenum disulfide and magnesium oxide nanoparticle performance on micropolar Cattaneo-Christov heat flux model*

M. G. REDDY[1], S. A. SHEHZAD[2,†]

1. Department of Mathematics, Acharya Nagarjuna University Campus,
Ongole 523001, Andhra Pradesh, India;

2. Department of Mathematics, COMSATS University Islamabad, Sahiwal 57000, Pakistan

Abstract This article intends to illustrate the Darcy flow and melting heat transmission in micropolar liquid. The major advantage of micropolar fluid is the liquid particle rotation through an independent kinematic vector named the microrotation vector. The novel aspects of the Cattaneo-Christov (C-C) heat flux and Joule heating are incorporated in the energy transport expression. Two different nanoparticles, namely, MoS_2 and MgO, are suspended into the base-fluid. The governing partial differential equations (PDEs) of the prevailing problem are slackening into ordinary differential expressions (ODEs) via similarity transformations. The resulting mathematical phenomenon is illustrated by the implication of fourth-fifth order Runge-Kutta-Fehlberg (RKF) scheme. The fluid velocity and temperature distributions are deliberated by using graphical phenomena for multiple values of physical constraints. The results are displayed for both molybdenum disulphide and magnesium oxide nanoparticles. A comparative benchmark in the limiting approach is reported for the validation of the present technique. It is revealed that the incrementing material constraint results in a higher fluid velocity for both molybdenum disulphide and magnesium oxide nanoparticle situations.

Key words micropolar fluid, Cattaneo-Christov (C-C) heat flux, molybdenum disulphide nanoparticle, melting effect, numerical solution

Chinese Library Classification O361
2010 Mathematics Subject Classification 76Sxx, 76Bxx

1 Introduction

Heat transport in distinct fluids has a wide range of implications in modern industrial and engineering developmental areas. It is necessary to save energy and time to overcome the limitations. Nowadays, many researchers and scholars are working on the fluids in the presence of nanoparticles called nanofluids. Choi and Eastman[1] first reported such work in this direction. They used combinations of different metals and metal oxides to obtain a

---

nano substance. By this research, it came to know that the heat transport performance of nanofluids is better than that of pure fluids such as water and oil. The idea of nanofluids made a revolutionary change in the field of research. Gholinia et al.[2] used silver and copper nanoparticles to illustrate the flow over a circular cylinder along with the electric conductivity. Ashjaee et al.[3] scrutinized the magnetohydrodynamic (MHD) ferrofluid flow to examine the pressure and heat drop in the system. Patel et al.[4] used the semi-analytic method to solve the micropolar fluid model with ferro-nanoparticles. Venkateswarlu et al.[5] illustrated the fluid temperature between MgO and MoS_2 water based nanofluids by considering the MHD and Cattaneo-Christov (C-C) heat flux over a sheet. Mohammad et al.[6] inspected a hybrid nanofluid over a porous medium with the effects of magnetic field and pressure gradient. Turkyilmazoglu[7] addressed both single and double phase nanofluid models in concentric annuli under slip mechanism. Mehryan et al.[8] described the magneto-hybrid nanofluid flow by considering the viscosity dependent on the magnetic field.

MHD flow has a wide range of applications in engineering, geophysics, astrophysics, study of earthquakes, aerospace engineering, and biological fields. The equations are the combination of Navier-Stokes and Maxwell equations. Turkyilmazoglu[9] described the magnetic field phenomena for mixed convected flows generated by a nonlinear deforming surface. Zeeshan et al.[10] scrutinized the MHD Couette-Poiseuille nanofluid flow by considering the activation energy along with the chemical reaction, and obtained the relation between concentration of the fluid and chemical reaction. The stagnation flow and the effect of Newtonian heating in the magnetic nanofluid over a surface were inspected by El-Haliem et al.[11]. Lu et al.[12] scrutinized the MHD Carreau nanofluid flow by applying a zero mass-flux condition. Khan et al.[13] considered the three-dimensional (3D) flow over two-directional stretching sheets, and used the Carreau rheological model. In the research of the magnetic effect, heat generation/absorption was taken into account. They revealed that the velocity is dependent on the Hartmann number. Reddy and Sandeep[14] explained the phenomena of MHD flow of Carreau nanofluid in the occupation of different effects.

Cattaneo[15] was the first person to change the Fourier heat conduction model by considering the time factor in heat transfer. Later, Christov[16] proposed the Maxwell-Cattaneo law which helped in eliminating heat flux and obtaining the single temperature equation. Straughan[17] continued the research on the C-C heat flux and explained the importance of higher Cattaneo numbers. Hayat et al.[18] illustrated a 3D flow under the C-C heat flux and used the optimal homotopy analysis method (OHAM) to obtain a solution. They showed that the temperature and concentration functions are inversely proportional to the relaxation parameter. Upadhya et al.[19] looked over the study of MHD fluid flow by considering dust and nanoparticles with the chemical reaction and C-C heat flux. Reddy[20] used the Oldroyd-B fluid to explain the significance and features of MHD flow over two different geometries with the C-C heat flux. The Runge-Kutta-Fehlberg (RKF) scheme was implemented to find the numerical solution. Mustafa[21] illustrated the C-C heat flux in a non-Newtonian fluid flow over a rotating system. Waqas et al.[22] illustrated the Burgers fluid flow with the C-C heat flux over a sheet. Hayat et al.[23] explained the C-C heat flux in the Maxwell fluid flow induced by a moving sheet.

Recently, Bakier[24] considered two types of flow to illustrate the melting effect in a porous medium over a plate. Cheng and Lin[25] scrutinized the mixed convection heat flux over a porous medium by considering the melting effect. Dinh et al.[26] considered the Lorentz force and melting effect on the MHD flow in a rotating system. Muhammad et al.[27] illustrated the heat transfer of a squeezing flow of hybrid nanofluids and nanofluids with viscous dissipation and melting effect, and revealed that the entropy generation is directly proportional to the squeezing, magnetic parameter, and Eckert number. Hayat et al.[28] illustrated the mixed convectional nanofluid flow in MHD over a stretchable plate with the melting effect. Kok[29] scrutinized heat transfer with or without fin in the presence of melting effect. Mehryan et al.[30] inspected the heat flow between vertical isothermal cylinders with the melting effect by using

the Galerkin finite element approach.

The literature review revealed that not much attention has been devoted to the magnetized micropolar fluid behaviors with suspension of molybdenum disulphide and magnesium nanoparticles induced by a melting sheet. Hence, the thermo-physical characteristics of the micro-polar non-Newtonian nanofluid over a melting sheet is expressed. The melting condition is developed for the execution of energy transmission of nanoparticles. The numerical scheme is adopted to visualize the results of modeled physical problem. The tabular and graphical descriptions are illustrated to express the behaviors of the problem. The results are also computed in a limiting approach to validate the methodology.

2 Modeling

The magnetized micropolar fluid flow induced by a melting surface with heat transmission is addressed. The melting sheet is stretched through a velocity $U_{\mathrm{w}}(x) = ax$. It is supposed that the melting sheet temperature is T_{m}, and the temperature at the free-stream is T_∞ such that $T_\infty \succ T_{\mathrm{m}}$. The wall temperature is assumed to be a constant, i.e., $T = T_\infty$. Further, the induced magnetic force is ignored due to a weaker magnetic Reynolds number. The physical illustration of the problem is shown in Fig. 1. The thermophysical values of nanofluids are demonstrated in Table 1.
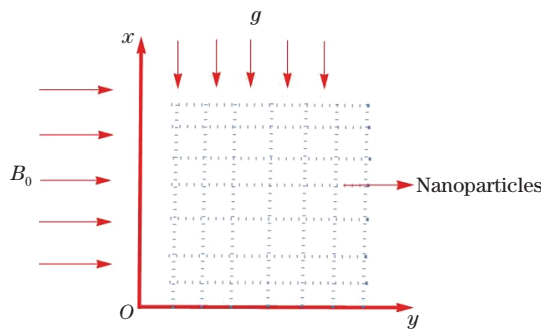

Fig. 1 Physical model of problem (color online)

Table 1 Thermo-physical properties of nanofluid

Property	Nanofluid
Density	$\rho_{\mathrm{nf}} = \phi\rho_{\mathrm{s}} + \rho_{\mathrm{f}}(1 - \phi)$
Viscosity	$\mu_{\mathrm{nf}} = \frac{\mu_{\mathrm{f}}}{(1-\phi)^{2.5}}$
Heat capacity	$(\rho c_p)_{\mathrm{nf}} = \phi(\rho c_p)_{\mathrm{s}} + (\rho c_p)_{\mathrm{f}}(1 - \phi)$
Thermal conductivity	$\frac{k_{\mathrm{nf}}}{k_{\mathrm{f}}} = \frac{2k_{\mathrm{f}}+k_{\mathrm{s}}-2(k_{\mathrm{f}}-k_{\mathrm{s}})\phi}{2k_{\mathrm{f}}+k_{\mathrm{s}}+2(k_{\mathrm{f}}-k_{\mathrm{s}})\phi}$
Heat conductivity	$1 + \frac{\left(\frac{\sigma_{\mathrm{s}}}{\sigma_{\mathrm{f}}}-1\right)3\phi}{\left(\frac{\sigma_{\mathrm{s}}}{\sigma_{\mathrm{f}}}+2\right)-\left(\frac{\sigma_{\mathrm{s}}}{\sigma_{\mathrm{f}}}-1\right)\phi}$

The formulated boundary layer equations of momentum and energy transfer expressions are written as[5–6,19–20]

$$\frac{\partial u}{\partial x} + \frac{\partial v}{\partial y} = 0, \tag{1}$$

$$u\frac{\partial u}{\partial x} + v\frac{\partial v}{\partial y} = \frac{1}{\rho_{\mathrm{nf}}}(\mu_{\mathrm{nf}} + \kappa)\frac{\partial^2 u}{\partial y^2} + \frac{\kappa}{\rho_{\mathrm{nf}}}\frac{\partial N}{\partial y} - \frac{\sigma_{\mathrm{nf}}}{\rho_{\mathrm{nf}}}B_0^2 u - g\beta_{\mathrm{nf}}(T - T_\infty), \tag{2}$$

$$j\Big(u\frac{\partial N}{\partial x} + v\frac{\partial N}{\partial y}\Big) = \frac{\gamma_{\mathrm{nf}}}{\rho_{\mathrm{nf}}}\frac{\partial^2 N}{\partial y^2} - \frac{\kappa}{\rho_{\mathrm{nf}}}\Big(2N + \frac{\partial u}{\partial y}\Big), \tag{3}$$

$$u\frac{\partial T}{\partial x} + v\frac{\partial T}{\partial y} = \frac{k_{\mathrm{nf}}}{(\rho c_p)_{\mathrm{nf}}}\frac{\partial^2 T}{\partial y^2} + \frac{\sigma_{\mathrm{nf}}}{\rho_{\mathrm{nf}}}B_0^2 u^2 + \lambda_1\Big(u\frac{\partial u}{\partial x}\frac{\partial T}{\partial x} + v\frac{\partial v}{\partial y}\frac{\partial T}{\partial y}$$
$$+ u\frac{\partial v}{\partial x}\frac{\partial T}{\partial y} + v\frac{\partial u}{\partial y}\frac{\partial T}{\partial x} + 2uv\frac{\partial^2 T}{\partial x\partial y} + u^2\frac{\partial^2 T}{\partial x^2} + v^2\frac{\partial^2 T}{\partial y^2}\Big), \tag{4}$$

in which u and v are the velocity components of fluid along the x- and y-coordinates, respectively, ρ_{nf} is the density of the nanofluid, μ_{nf} is the dynamic viscosity, κ is the vortex viscosity, N is the micro rotation, σ_{nf} is the electrical conductivity, ν_{nf} is the kinematic viscosity, j is the micro rotation density, T is the temperature, γ_{nf} is the spin gradient viscosity, B_0 is the strength of magnetic field, c_p is the specific heat capacity, and λ_1 is the parameter of thermal relaxation.

The appropriate conditions for the considered flow situation are

$$\begin{cases} u = U_{\mathrm{w}}(x), \quad v = 0, \quad N = -\delta^*\dfrac{\partial u}{\partial y}, \quad T = T_{\mathrm{m}}, \\[2mm] k_{\mathrm{nf}}\Big(\dfrac{\partial T}{\partial y}\Big) = \rho_{\mathrm{nf}}(\lambda + C_{\mathrm{s}}(T_{\mathrm{m}} - T_{\mathrm{s}}))v(x,0) \quad \text{at} \quad y = 0, \end{cases} \tag{5a}$$

$$u \to 0, \quad v \to 0, \quad T \to T_\infty \quad \text{as} \quad y \to \infty, \tag{5b}$$

where δ^* is the melting constant, and its value lies between $0 \leqslant \delta^* \leqslant 1$.

Introduce the following similarity transformations:

$$u = axf'(\eta), \quad v = -\sqrt{a\nu_{\mathrm{f}}}f(\eta), \quad \eta = \sqrt{\frac{a}{\nu_{\mathrm{f}}}}y, \quad N = ax\sqrt{\frac{a}{\nu_{\mathrm{f}}}}g(\eta), \quad \theta = \frac{T - T_{\mathrm{m}}}{T_\infty - T_{\mathrm{m}}}. \tag{6}$$

Then, Eq. (1) is satisfied automatically, while Eqs. (2)–(4) can be reduced as follows:

$$\Big(\frac{1}{(1-\phi)^{2.5}} + K\Big)f''' + \Big(1 - \phi + \phi\frac{\rho_{\mathrm{s}}}{\rho_{\mathrm{f}}}\Big)ff'' - M\Big(1 + \frac{3(\frac{\sigma_{\mathrm{s}}}{\sigma_{\mathrm{f}}} - 1)\phi}{(\frac{\sigma_{\mathrm{s}}}{\sigma_{\mathrm{f}}} + 2) - (\frac{\sigma_{\mathrm{s}}}{\sigma_{\mathrm{f}}} - 1)\phi}\Big)f'$$
$$- \Big(1 - \phi + \phi\frac{\rho_{\mathrm{s}}}{\rho_{\mathrm{f}}}\Big)f'^2 + \lambda_2\theta = 0, \tag{7}$$

$$\Big(\frac{1}{(1-\phi)^{2.5}} + \frac{K}{2}\Big)g'' + \Big(1 - \phi + \phi\frac{\rho_{\mathrm{s}}}{\rho_{\mathrm{f}}}\Big)fg' - \Big(1 - \phi + \phi\frac{\rho_{\mathrm{s}}}{\rho_{\mathrm{f}}}\Big)f'g - K(2g + f'') = 0, \tag{8}$$

$$\frac{1}{Pr}\Big(\frac{k_{\mathrm{s}} + 2k_{\mathrm{f}} - 2\phi(k_{\mathrm{f}} - k_{\mathrm{s}})}{k_{\mathrm{s}} + 2k_{\mathrm{f}} + \phi(k_{\mathrm{f}} - k_{\mathrm{s}})}\Big)\theta'' + \Big(1 - \phi + \phi\frac{(\rho c_p)_{\mathrm{s}}}{(\rho c_p)_{\mathrm{f}}}\Big) + \delta_1(ff'\theta' + f\theta'')$$
$$\cdot \Big(1 + \frac{3(\frac{\sigma_{\mathrm{s}}}{\sigma_{\mathrm{f}}} - 1)\phi}{(\frac{\sigma_{\mathrm{s}}}{\sigma_{\mathrm{f}}} + 2) - (\frac{\sigma_{\mathrm{s}}}{\sigma_{\mathrm{f}}} - 1)\phi}\Big)MEcf'^2 = 0. \tag{9}$$

The transformed conditions are

$$\begin{cases} f'(0) = 1, \quad f(0) = 0, \quad g(0) = -\delta^* f''(0), \\[2mm] \dfrac{k_{\mathrm{nf}}}{k_{\mathrm{f}}}M_1\theta'(0) + \Big(1 - \phi + \dfrac{\rho_{\mathrm{nf}}}{\rho_{\mathrm{f}}}\phi\Big)PrF(0) = 0, \quad \theta(0) = 0 \quad \text{at} \quad \eta = 0, \end{cases} \tag{10a}$$

$$f'(\infty) \to 0, \quad g(\infty) \to 0, \quad \theta(\infty) \to 1 \quad \text{as} \quad \eta \to \infty, \tag{10b}$$

in which $K = \frac{\kappa}{\mu_{\mathrm{f}}}$ is the material parameter, $j = \frac{\nu_{\mathrm{f}}}{a}$ is the micro rotation density, $M = \frac{\sigma_{\mathrm{f}}B_0^2}{a\rho_{\mathrm{f}}}$ is the magnetic parameter, $Pr = \frac{(\rho c_p)\nu_{\mathrm{f}}}{k_{\mathrm{f}}}$ is the Prandtl number, $Ec = \frac{u_{\mathrm{w}}^2}{c_p(T_\infty - T_{\mathrm{m}})}$ is the Eckert

number, $\lambda_2 = \frac{Gr_x}{Re_x^2}$ is the thermal buoyancy parameter, $Gr_x = \frac{g\beta_{nf}(T_\infty - T_m)x^3}{\nu^2}$ is the local thermal Grashof number, $Re_x = \frac{U_w x}{\nu}$ is the local Reynolds number, $M_1 = \frac{T_\infty - T_m}{c_p(\lambda + C_s(T_m - T_s))}$ is the melting parameter with C_s being the heat capacity of the solid surface and T_s being the solid temperature, and $\delta_1 = \lambda_1 a$ is the non-dimensional Deborah number. Note that the present flow analysis constrains to the hydrodynamic case by setting $M = 0$.

The dimensionless forms of the drag force and the heat transmission rate are addressed as

$$C_{fx} = \frac{\tau_w}{\rho_f U_w^2}, \quad Nu_x = \frac{xq_w}{k_f(T_\infty - T_m)},$$

where τ_w and q_w are defined as

$$\tau_w = (\mu_{nf} + \kappa)\frac{\partial u}{\partial y} + \kappa N\Big|_{y=0},$$

$$q_w = -k_{nf}\frac{\partial T}{\partial y}\Big|_{y=0} + (q_r)_w,$$

in which $C_{fx}Re_x^{1/2}$ and $Nu_x Re_x^{-1/2}$ are defined as

$$C_{fx}Re_x^{1/2} = \Big(\frac{1}{(1-\phi)^{2.5}} + K(1-\delta^*)\Big)f''(0),$$

$$Nu_x Re_x^{-1/2} = -\frac{k_{nf}}{k_f}\theta'(0).$$

3 Solution procedure

In this part, the nonlinear ordinary differential expressions (ODEs) (7)–(9) with the prescribed condition (10) are calculated numerically by engaging the RKF technique using MATLAB. The major advantage of this method is its efficiency and easy implementation. This method is self-starting and stable unlike other multi-step techniques. In this context, the boundary value is developed into the initial value.

$$\begin{cases} f = y_1, \quad f' = y_2, \quad f'' = y_3, \\ f''' = \dfrac{(1-\phi)^{2.5}}{1 + K(1-\phi)^{2.5}}\Big(-\Big(1 + \dfrac{\rho_s}{\rho_f}\phi - \phi\Big)y_1 y_3\Big) + \Big(1 + \dfrac{\rho_s}{\rho_f}\phi - \phi\Big)y_2^2 \\ \qquad + M\Big(1 + \dfrac{\big(\frac{\sigma_s}{\sigma_f} - 1\big)3\phi}{\big(2 + \frac{\sigma_s}{\sigma_f}\big) - \big(\frac{\sigma_s}{\sigma_f} - 1\big)\phi}\Big)y_2 - \lambda_2 y_6, \end{cases} \tag{11}$$

$$\begin{cases} g = y_4, \quad g' = y_5, \\ g'' = \dfrac{2(1-\phi)^{2.5}}{2 + K(1-\phi)^{2.5}}\Big(-\Big(1 + \dfrac{\rho_s}{\rho_f}\phi - \phi\Big)y_1 y_5 + \Big(1 + \dfrac{\rho_s}{\rho_f}\phi - \phi\Big)y_2 y_4 + K(2y_4 + y_3)\Big), \end{cases} \tag{12}$$

$$\begin{cases} \theta = y_6, \quad \theta' = y_7, \\ \theta'' = \Big(\dfrac{Pr(k_s + 2k_f + \phi(k_f - k_s))}{k_s + 2k_f + \delta_1 y_1(k_s + 2k_f + \phi(k_f - k_s) - 2\phi(k_f - k_s))}\Big) \\ \qquad + \Big(1 + \phi\dfrac{(\rho c_p)_s}{(\rho c_p)_f} - \phi\Big)y_1 y_7 + \Big(1 + \dfrac{\big(\frac{\sigma_s}{\sigma_f} - 1\big)3\phi}{\big(2 + \frac{\sigma_s}{\sigma_f}\big) - \big(\frac{\sigma_s}{\sigma_f} - 1\big)\phi}\Big)MEcy_2^2 + \delta_1 y_1 y_2 y_7. \end{cases} \tag{13}$$

The transformed boundary conditions are

$$
\begin{cases}
y_2 = 1, \quad y_1 = 0, \quad y_4 = -\delta^* y_3, \\
\dfrac{k_{\mathrm{nf}}}{k_{\mathrm{f}}} M_1 y_7 + \left(1 - \phi + \dfrac{\rho_{\mathrm{nf}}}{\rho_{\mathrm{f}}} \phi\right) Pr y_1 = 0, \quad y_6 = 0 \quad \text{at} \quad \eta = 0,
\end{cases}
\tag{14a}
$$

$$
y_2 \to 0, \quad y_4 \to 0, \quad y_6 \to 1 \quad \text{as} \quad \eta \to \infty.
\tag{14b}
$$

To solve Eqs. (11)–(13), we adopt y_3, y_5, and y_7 which are not given at the prior conditions. Later, the prior stages are declared by using the RKF method with the subsequent looping step of length 0.01.

4　Graphical analysis

The steady flow and heat transport of micropolar fluid over a melting sheet are investigated. Two types of oxides, namely, molybdenum disulphide and magnesium oxides, are suspended into the base-fluid water. The mixed convection heat transmission with the melting effect is described. The numerical mechanism, namely, the RKF fourth-fifth order together with the shooting scheme, is adopted to exploit the dimensionless modeled expressions of the current problem. The effects of various governing parameters on $f'(\eta)$, $h(\eta)$, and $\theta(\eta)$ are demonstrated graphically. The present study is also compared with the available results of Venkateswarlu et al.[5] and Reddy and Sandeep[14] (see Table 2). The limiting results are in good match with each other.

**Table 2** Comparison data of skin friction coefficient with Venkateswarlu et al.[5] and Reddy and Sandeep[14]

M	$-f''(0)$		
	Venkateswarlu et al.[5]	Reddy and Sandeep[14]	Present
1	–1.414 21	1.414 21	–1.411 23
5	–2.449 49	2.449 80	–2.449 87
10	–3.316 62	3.316 62	–3.316 76
50	–7.141 43	7.141 42	–7.134 52

### 4.1　Fluid velocity $f'(\eta)$

Figures 2–6 execute the behaviors of the fluid velocity profiles against different physical parametric values. Figure 2 represents the nature of M on the velocity $f'(\eta)$ profile. Here, it is achieved that higher values of M augment the fluid velocity. The compactness of the corresponding momentum layer rises for the improving trend of M. Physically, a larger M implies stronger Lorentz forces. The improvement in the Lorentz force generates more drag to resist the liquid flow. The influence of the material parameter on the velocity profile $f'(\eta)$ for both MoS$_2$ and MgO nanoparticle cases is depicted in Fig. 3. Here, the incrementing nature of K booms the velocity $f'(\eta)$ and compactness of momentum layer also cultivate for growing values of K. Furthermore, the enhancement of fluid flow is higher in MgO nanoparticle situation than that in MoS$_2$ nanoparticle situation. The connections of the buoyancy parameter λ_2 on $f'(\eta)$ for both MoS$_2$ and MgO nanoparticle cases are visualized in Fig. 4. Here, it is observed that the uplifting values of λ_2 scale back the fluid flow in both nanoparticle cases. Additionally, the thicker momentum boundary layer is achieved for larger λ_2. Further, the fluid velocity is more dropped in MgO nanoparticles when compared with MoS$_2$ nanoparticle case. Figure 5 exhibits the nanoparticle volume fraction ϕ behavior on $f'(\eta)$. It is perceived that the increment in ϕ improves the fluid velocity for both cases. The influence of the melting parameter on the velocity profile $f'(\eta)$ for both MoS$_2$ and MgO nanoparticle cases is illustrated through Fig. 6. It is mentioned that the larger integrities of M_1 rise the velocity of the fluid.
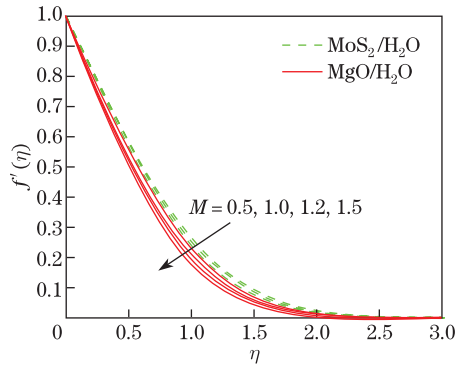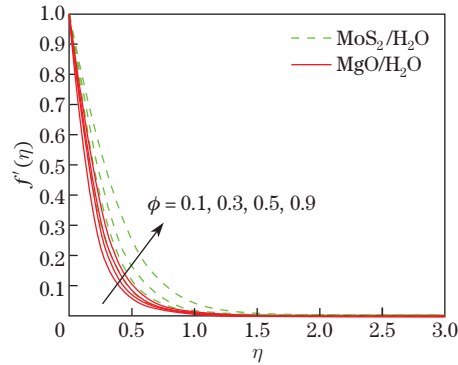
Fig. 2   Behaviors of M on $f'(\eta)$ (color online)
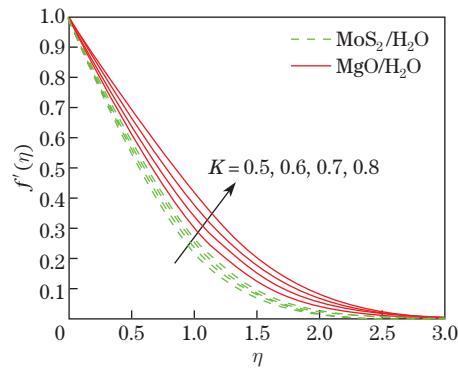
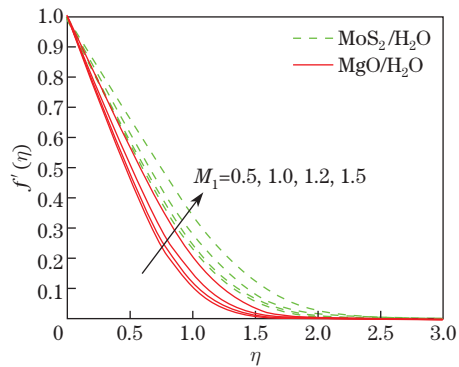**Fig. 3**   Behaviors of K on $f'(\eta)$ (color online)
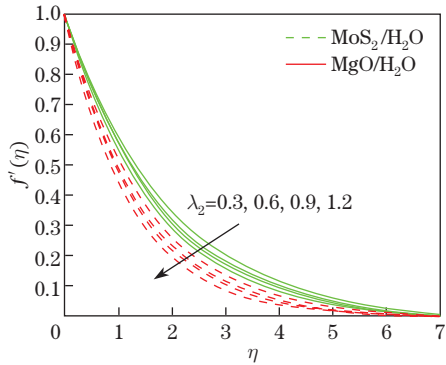
Fig. 4   Behaviors of λ_2 on $f'(\eta)$ (color online)


Fig. 5   Behaviors of ϕ on $f'(\eta)$ (color online)

4.2   Angular velocity $g(\eta)$

In Fig. 7, the angular velocity distribution $g(\eta)$ is presented for different values of the material parameter K for both MoS_2 and MgO nanoparticle cases. One may observe from this figure that the angular fluid velocity enhances for improving values of K. The momentum layer of both MoS_2 and MgO nanoparticle cases enhances for booming values of the material parameter. Additionally, the enhancement in the angular fluid flow is higher for MoS_2 nanoparticle case as compared to MgO nanoparticle case. The microrotation parameter δ^* aspects on the

Fig. 6   Behaviors of M_1 on $f'(\eta)$ (color online)
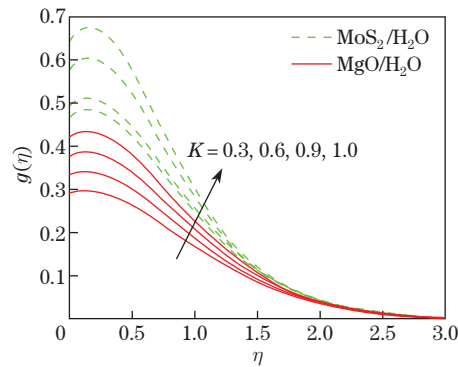
Fig. 7   Behaviors of K on $g(\eta)$ (color online)

angular fluid velocity $g(\eta)$ distribution are observed in Fig. 8. A decrement in microrotation for both MoS_2 and MgO nanoparticle cases is achieved for enlarging δ^*. Figure 9 exhibits the nanoparticle volume fraction ϕ on the angular velocity profile $g(\eta)$. The expanding values of ϕ boost the angular fluid velocity and the corresponding boundary layer for both nanoparticle cases.
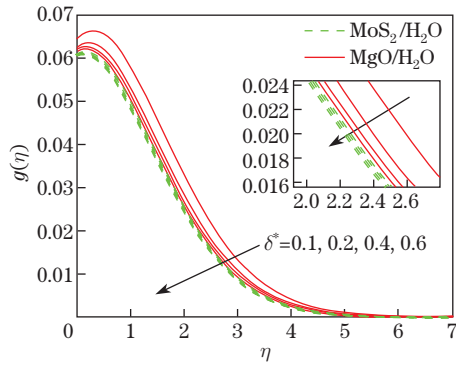

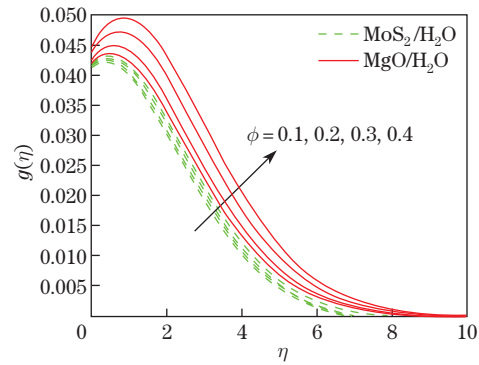**Fig. 8**   Behaviors of δ^* on $g(\eta)$ (color online)

Fig. 9   Behaviors of ϕ on $g(\eta)$ (color online)

4.3   Temperature profile $\theta(\eta)$

Figure 10 reports the temperature profiles $\theta(\eta)$ for both MoS_2 and MgO nanoparticle cases against varying Prandtl numbers Pr. The temperature profile and thermal layer decay for incrementing Pr. Physically, the melting aspect for advanced values of Pr has lower thermal diffusivity. Finally, larger values of Pr scale back the fluid temperature. The domination of nanoparticle volume fractions on $\theta(\eta)$ for MoS_2 and MgO nanoparticle cases is distinguished through Fig. 11. It is mentioned that the larger ϕ rises the temperature of the fluid. Physically, the increment in ϕ results in stronger thermal conductance of the material which returns to boost the fluid temperature. Figure 12 demonstrates the variations of $\theta(\eta)$ against higher melting parameters. The larger values of M_1 lead to a reduction in the nanofluid temperature for both MoS_2 and MgO nanoparticle cases. Indeed, more advanced M_1 values escort to more convected flow from the melting sheet towards the hot fluid. It follows that the fluid temperature is dropped. Figure 13 demonstrates the changes in $\theta(\eta)$ for the Eckert number Ec. As conventional, hotness of the fluid and compactness of thermal layer dwindle for both MoS_2 and MgO nanoparticle cases for higher values of Ec. In Fig. 14, the temperature distribution $\theta(\eta)$ is presented for different values of δ_1 for both MoS_2 and MgO nanoparticle cases. The
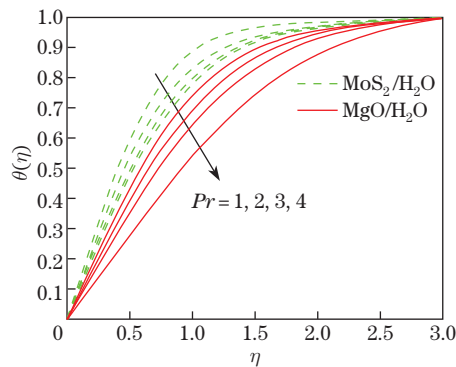

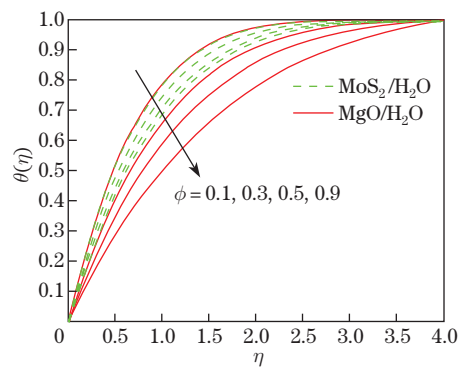**Fig. 10**   Behaviors of Pr on $\theta(\eta)$ (color online)
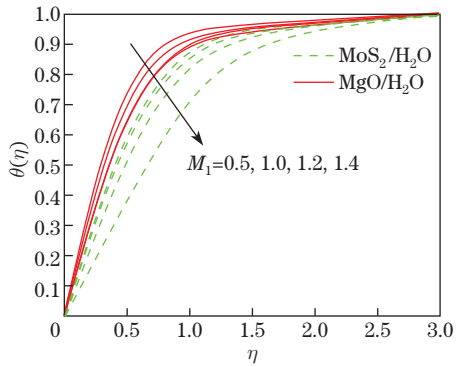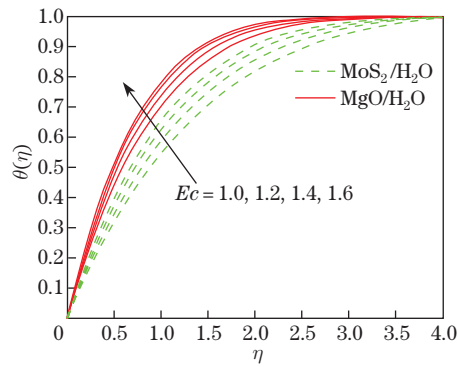
Fig. 11   Behaviors of ϕ on $\theta(\eta)$ (color online)

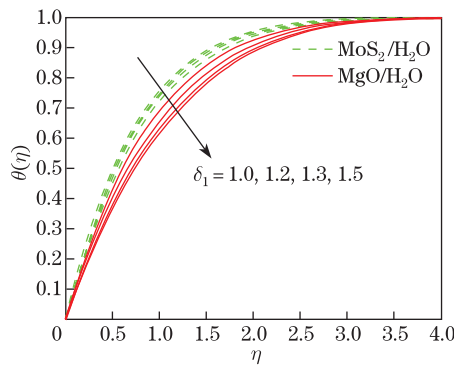**Fig. 12** Behaviors of M_1 on $\theta(\eta)$ (color online)

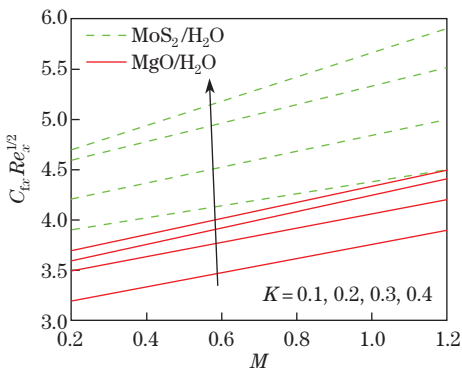**Fig. 13** Behaviors of Ec on $\theta(\eta)$ (color online)

incrementing trend of δ_1 values leads to weaker fluid temperature for both MoS_2 and MgO nanoparticle cases.

4.4 Friction factor and Nusselt number

Figure 15 describes the variations in $C_{fx}Re_x^{1/2}$ for varying magnetic and material parameters. Here, the improving magnetic constraint enhances $C_{fx}Re_x^{1/2}$, and a similar trend is observed for enhancing the material parameter values. The role of M_1 and Pr on $Nu_xRe_x^{-1/2}$ is demonstrated through Fig. 16. This figure illustrates that higher values of M_1 and Pr increase $Nu_xRe_x^{-1/2}$ for both MoS_2 and MgO nanoparticle cases.

Fig. 14 Behaviors of δ_1 on $\theta(\eta)$ (color online)

Fig. 15 Behaviors of M and K on $C_{fx}Re_x^{1/2}$ (color online)
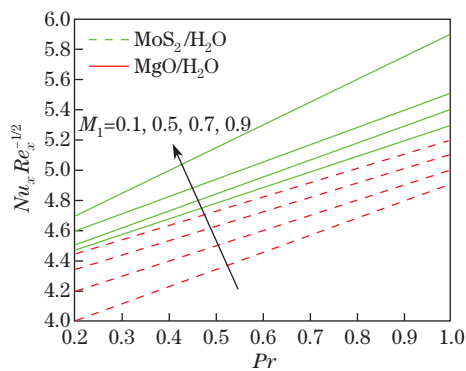
Fig. 16 Behaviors of Pr and M_1 on $Nu_xRe_x^{-1/2}$ (color online)

The phenomenon of diversity of flow constraints on $Re_x^{1/2}C_{\mathrm{f}x}$ and $Re_x^{-1/2}Nu_x$ is illustrated in Table 3. The friction coefficient enhances by increasing M, λ_2, Pr, and δ_1, but a reverse tendency is observed for magnifying K, ϕ, δ^*, and M_1. Furthermore, the heat transmission rate values are exaggerated by accumulating the values of Pr, M_1, K, and ϕ, but a reverse trend is seen for λ_2, δ_1, and Ec.

Table 3 Numerical values of $Re_x^{1/2}C_{\mathrm{f}x}$ and $Re_x^{-1/2}Nu_x$ for different values of $K, M, M_1, \lambda_2, Pr, \delta^*, Ec, \delta_1$, and ϕ

K	M	λ_2	Pr	δ_1	Ec	ϕ	δ^*	M_1	Friction factor coefficient	Nusselt number
0.2									0.983 24	0.309 91
0.3									0.977 65	0.311 33
0.4									0.968 52	0.322 34
	0.5								1.213 23	0.269 78
	1.0								1.223 14	0.311 25
	1.5								1.241 22	0.323 41
		0.3							1.156 74	0.523 45
		0.5							1.189 02	0.521 09
		0.7							1.200 45	0.511 23
			2						1.000 92	0.329 43
			3						1.013 21	0.378 65
			4						1.120 94	0.401 88
				0.4					1.213 22	0.534 21
				0.6					1.221 34	0.523 34
				0.8					1.342 10	0.512 32
					1.1				0.955 43	0.483 31
					1.2				0.953 42	0.456 72
					1.3				0.944 32	0.445 78
						0.1			0.899 00	0.733 21
						0.2			0.711 21	0.741 23
						0.3			0.643 21	0.744 56
							0.2		1.098 21	0.711 20
							0.4		0.001 23	0.812 54
							0.6		0.000 09	0.982 34
								0.7	0.889 21	0.622 10
								0.9	0.876 61	0.711 09
								1.1	0.866 98	0.898 90

5 Conclusions

The molybdenum disulphide and magnesium oxide nanoparticle performance through C-C heat flux and melting process in magneto-micro nanofluid is studied. The outcomes of the velocity and temperature profiles for MoS_2 and MgO nanoparticle cases against various non-dimensional parametric values are presented graphically. Based on the tabulated and graphical results, we extract the following conclusions.

(i) The velocity profile rises up with ϕ, M_1, and K, but a decay trend is noticed against improving values of M and λ_2.

(ii) The temperature profile increases with mounting values of Ec while decreases with augmented Pr, M_1, and δ_1.

(iii) The skin friction coefficient rises up against higher values of M, λ_2, Pr, and δ_1 while decreases for larger values of K, ϕ, δ^*, and M_1.

(iv) The Nusselt number is magnified with boosting values of Pr, M_1, K, and ϕ while decreases for increasing values of λ_2, δ_1, and Ec.

References

[1] CHOI, S. U. S. and EASTMAN, J. A. Enhancing thermal conductivity of fluids with nanoparticles. *ASME-Publications-Fed*, **231**, 99–106 (1995)

[2] GHOLINIA, M., GHOLINIA, S., HOSSEINZADEH, K., and GANJI, D. D. Investigation on ethylene glycol nanofluid flow over a vertical permeable circular cylinder under effect of magnetic field. *Results in Physics*, **9**, 1525–1533 (2018)

[3] ASHJAEE, M., GOHARKHAH, M., KHADEM, L. A., and AHMADI, R. Effect of magnetic field on the forced convection heat transfer and pressure drop of a magnetic nanofluid in a miniature heat sink. *Heat and Mass Transfer*, **51**, 953–964 (2015)

[4] PATEL, R. H., MITTAL, S. A., and DARJI, R. R. MHD flow of micropolar nanofluid over a stretching/shrinking sheet considering radiation. *Internal Communications in Heat and Mass Transfer*, **108**, 104322 (2019)

[5] VENKATESWARLU, S., VARMA, S. V., and PRASAD, P. D. MHD flow of MoS_2 and MgO water-based nanofluid through porous medium over a stretching surface with Cattaneo-Christov heat flux model and convective boundary condition. *International Journal of Ambient Energy*, (2020) https://doi.org/10.1080/01430750.2020.1785939

[6] MOHAMMAD, G., SABOUR, M., POP, I., and WEN, D. S. Free convection heat transfer of MgO-MWCNTs/EG hybrid nanofluid in a porous complex shaped cavity with MHD and thermal radiation effects. *International Journal of Numerical Methods for Heat and Fluid Flow*, **29**, 4349–4376 (2019)

[7] TURKYILMAZOGLU, M. Fully developed slip flow in a concentric annuli via single and dual phase nanofluids models. *Computer Methods and Programs in Biomedicine*, **179**, 104997 (2019)

[8] MEHRYAN, S. A. M., IZADI, M., NAMAZIAN, Z., and CHAMKHA, A. J. Natural convection of multi-walled carbon nanotube-Fe_3O_4/water magnetic hybrid nanofluid flowing in porous medium considering the impacts of magnetic field-dependent viscosity. *Journal of Thermal Analysis and Calorimetry*, **138**, 1541–1555 (2019)

[9] TURKYILMAZOGLU, M. Analytical solutions to mixed convection MHD fluid flow induced by a nonlinearly deforming permeable surface. *Communications in Nonlinear Science and Numerical Simulation*, **63**, 373–379 (2018)

[10] ZEESHAN, A., SHEHZAD, N., and ELLAHI, R. Analysis of activation energy in Couette-Poiseuille flow of nanofluid in the presence of chemical reaction and convective boundary conditions. *Results in Physics*, **8**, 502–512 (2018)

[11] EL-HALIEM, M. A., RAMZAN, M., and CHUNG, J. D. A numerical study of magnetohydrodynamic stagnation point flow of nanofluid with Newtonian heating. *Journal of Computational and Theoretical NanoScience*, **13**, 8419–8426 (2016)

[12] LU, D., RAMZAN, M., HUDA, N. U., CHUNG, J. D., and FAROOQ, U. Nonlinear radiation effect on MHD Carreau nanofluid flow over a radially stretching surface with zero mass flux at the surface. *Scientific Reports*, **8**, 3709 (2018)

[13] KHAN, M., HUMARA, S., and HASHIM. Heat generation/absorption and thermal radiation impacts on three dimensional flow of Carreau fluid with convective heat transfer. *Journal of Molecular Liquids*, **18**, 474–480 (2018)

[14] REDDY, M. G. and SANDEEP, N. Heat and mass transfer in radiative MHD Carreau fluid with cross diffusion. *Ain Shams Engineering Journal*, **9**, 1189–1204 (2018)

[15] CATTANEO, C. Sulla conduzionedelcalore. *Atti del Seminario Matematico e Fisico dell Universita di Modena e Reggio Emilia*, **3**, 83–101 (1948)

[16] CHRISTOV, C. I. On frame indifferent formulation of the Maxwell-Cattaneo model of finite-speed heat conduction. *Mechanics Research Communications*, **36**, 481–486 (2009)

[17] STRAUGHAN, B. Thermal convection with the Cattaneo-Christov model. *International Journal of Heat and Mass Transfer*, **53**, 95–98 (2010)

[18] HAYAT, T., AZIZ, A., MUHAMMAD, T., and ALSAEDI, A. Three-dimensional flow of Prandtl fluid with Cattaneo-Christov double diffusion. *Results in Physics*, **9**, 290–296 (2018)

[19] UPADHYA, S. M., RAJU, C. S. K., MAHESHA, and SALEEM, S. Nonlinear unsteady convection on micro and nanofluid with Cattaneo-Christov heat flux. *Results in Physics*, **9**, 779–786 (2018)

[20] REDDY, M. G. Cattaneo-Christov heat flux effect on hydromagnetic radiative Oldroyd-B liquid flow across a cone/wedge in the presence of cross-diffusion. *The European Physical Journal Plus*, **133**, 24 (2018)

[21] MUSTAFA, M. Cattaneo-Christov heat flux model for rotating flow and heat transfer of upper convected Maxwell fluid. *AIP Advances*, **5**, 47–109 (2015)

[22] WAQAS, M., HAYAT, T., FAROOQ, M., SHEHZAD, S. A., and ALSAEDI, A. Cattaneo-Christov heat flux model for flow of variable thermal conductivity generalized Burgers fluid. *Journal of Molecular Liquids*, **220**, 642–648 (2016)

[23] HAYAT, T., FAROOQ, M., ALSAEDI, A., and AL-SOLAMY, F. Impact of Cattaneo-Christov heat flux in the flow over a stretching sheet with variable thickness. *AIP Advances*, **5**, 87–159 (2016)

[24] BAKIER, A. Y. Aiding and opposing mixed convection flow in melting from a vertical flat plate embedded in a porous medium. *Transport in Porous Media*, **29**, 127–139 (1997)

[25] CHENG, W. T. and LIN, C. H. Melting effect on mixed convective heat transfer with aiding and opposing external flows from the vertical plate in a liquid-saturated porous medium. *International Journal of Heat and Mass Transfer*, **50**, 3026–3034 (2007)

[26] DINH, M. T., TLILI, I., DARA, R. N., SHAFEE, A., AL-JAHMANY, Y. Y. Y., and NGUYEN-THOI, T. Nanomaterial treatment due to imposing MHD flow considering melting surface heat transfer. *Physica A*: *Statistical Mechanics and its Applications*, **541**, 123036 (2020)

[27] MUHAMMAD, K., HAYAT, T., ALSAEDI, A., and AHMAD, B. Melting heat transfer in squeezing flow of basefluid (water), nanofluid (CNTs+water) and hybrid nanofluid (CNTs+CuO+water). *Journal of Thermal Analysis and Calorimetry*, **143**, 1157–1174 (2021)

[28] HAYAT, T., SHAH, F., ALSAEDI, A., and AHMAD, B. Entropy optimized dissipative flow of effective Prandtl number with melting heat transport and Joule heating. *International Communications in Heat and Mass Transfer*, **111**, 104454 (2020)

[29] KOK, B. Examining effects of special heat transfer fins designed for the melting process of PCM and nano-PCM. *Applied Thermal Engineering*, **170**, 114989 (2020)

[30] MEHRYAN, S. A. M., VAEZI, M., SHEREMET, M., and GHALAMBAZ, M. Melting heat transfer of power-law non-Newtonian phase change nano-enhanced n-octadecane-mesoporous silica (MPSiO$_2$). *International Journal of Heat and Mass Transfer*, **151**, 119385 (2020)